

# **High power transcranial beam steering for ultrasonic brain therapy**

M. Pernot, J.-F. Aubry, M. Tanter, J.-L. Thomas and M. Fink.

Laboratoire Ondes et Acoustique, ESPCI, Université Paris VII,  
U.M.R C.N.R.S. 7587, 10 rue Vauquelin, 75005 Paris, France

Shortened title: High power ultrasonic array for brain therapy.

## **Abstract**

A sparse phased array is specially designed for non-invasive ultrasound transskull brain therapy. The array is made of 200 single-elements corresponding to a new generation of high power transducers developed in collaboration with Imasonic (Besançon, France). Each element has a surface of  $0.5\text{cm}^2$  and works at 0.9 MHz central frequency with a maximum  $20\text{W}\cdot\text{cm}^{-2}$  intensity on the transducer surface. In order to optimize the steering capabilities of the array, several transducers distributions on a spherical surface are simulated: hexagonal, annular, and quasi-random distributions. Using a quasi-random distribution significantly reduces the grating lobes. Furthermore, the simulations show the capability of the quasi-random array to electronically move the focal spot in the vicinity of the geometrical focus (up to  $\pm 15$  mm). Based on the simulation study, the array is constructed and tested. The skull aberrations are corrected by using a time reversal mirror with amplitude correction achieved thanks to an implantable hydrophone, and a sharp focus is obtained through a human skull. Several lesions are induced in fresh liver and brain samples through human skulls, demonstrating the accuracy and the steering capabilities of the system.

## 1. Introduction

The effects of High Intensity Focused Ultrasound (HIFU) in human and animal brains have been extensively investigated (Fry *et al.* 1955, Basauri and Lele 1962, Dunn and Fry 1971, Robinson and Lele 1972, Fry *et al.* 1986, Vykhodtseva *et al.* 1994), and these studies have shown the feasibility of ultrasound brain therapy and surgery with the skull bone removed. However non invasive transskull therapy remains very limited due to the strong phase aberrations and absorption induced by the skull, as was first shown by Fry and Barger (1978). To compensate for this distortion, Phillips *et al.* (1975) introduced the idea of phased array corrections to ultrasound diagnostic imaging through the skull. In 1996, Thomas and Fink proposed to use a time reversal mirror in therapeutic ultrasound. Prior to the treatment and taking advantage of the biopsy, which ensures that the tumor is malignant, one could put a hydrophone in the neighborhood of the tumor and record the signals relating this hydrophone to each element of the therapeutic array. Once the diagnosis has been confirmed and the hydrophone removed, one would have to emit the time reversed signals with amplitude compensation in order to correct for both phase and amplitude aberrations induced by the skull. They validated this technique experimentally at low amplitude levels, showing a strong improvement of up to 10 dB in focus quality. In 1998, Hynynen *et al.* have applied a similar phase conjugation technique (equivalent to time reversal process for monochromatic signals) with a high intensity ultrasound system. Recently several studies have shown that this reliable and minimally invasive procedure could be replaced by a totally non-invasive method that uses MRI (Sun and Hynynen 1998) or CT images (Pernot *et al.* 2001, Clement and Hynynen 2002, Aubry *et al.* 2003) to predict the aberrations that will be induced by the skull.

In order to steer the beam electronically and heat the whole target spot by spot without moving the therapeutic array, Tanter *et al.* proposed in 1998 combining the time reversal

process with a numerical back-propagation and steering algorithm, and demonstrated experimentally its feasibility at low intensities. Recently, Clement *et al.* (2002) used a similar steering technique at high power to achieve in vitro necrosis at the geometrical center of the array with a beam steered from an implantable hydrophone located 1cm away. However, as explained in their article, the beamwidths of the elements were too tight to obtain a good beam focusing outside of the geometrical center and the array only permitted the restoration of the focus with enough power at the geometrical center. They concluded that a significant improvement in the steering range would occur by using much smaller elements. The present study demonstrates that a significant power at the focus and high precision focusing and steering capabilities can be obtained with a reasonable number of transducers.

In order to build an array that can correct for these aberrations, a number of design considerations such as the number of elements, the aperture and the frequency, have been previously discussed by Clement *et al* (2000). Based on different considerations on the beam steering capabilities, we put our efforts to design a new prototype that used the great versatility of single-element technology. In close collaboration with Imasonic (Besançon, France) we have developed a new technology of high power elements with small diameter that can be distributed on any surface. Such a technology enables to control completely the shape and the size of the array active surface. Moreover the large bandwidth of this single-element technology enables to work between 0.7 and 1.1 MHz. All the single-elements are embedded in homemade moulds resulting in an easily upgradeable system. The number of elements results from several compromises: the energy must be distributed over a large area of the skull in order to reach the maximum antenna gain and avoid undesired skull heating, but at the same time the size of the transducers elements should be small compared to the correlation length of the skull in order to achieve a good correction of the

skull aberrations. Moreover the steering capabilities of the array and the grating lobes are strongly related to the size and inter-element distance of the transducers. Finally the cost of the system increases with the number of transducers and has to be taken into consideration.

However, an important disadvantage of large phased arrays is the unwanted presence of grating lobes, and the need to reduce the grating lobes has been common to all therapeutic arrays reported to date (Dupenloup *et al.* 1996, Lockwood and Foster 1996). Goss *et al.* (1996), Gavrilov and Hand (2000), have shown theoretically that the use of elements randomly distributed on a segment of a spherical surface may improve the performances of a phased array, particularly the focusing quality when the focus is moved electronically in the vicinity of the geometrical center.

In this study such a large sparse array is specially designed for transskull brain therapy. It is optimized both for correcting the skull aberrations and for its beam steering capabilities. The electronic conception of the multi-channel system represents an important progress since 200 high power emission boards and 100 independent reception boards are available for positioning and imaging before and during the heating sequence. The performance of several transducers distributions (hexagonal, annular and quasi-random distribution) has been investigated in order to minimize the grating lobes, and maximize the region in which the focus can be successfully moved. Based on the simulation, the array has been constructed and experimental results are shown. This new device presents very good performances in terms of aberration correction capabilities, electronic beam steering and power level. Finally these performances are experimentally demonstrated by thermally inducing precise lesions through human skulls in fresh liver and brain samples.

## 2. Array Design and specifications

A 900 kHz central frequency has been chosen for the array by considering several factors: the aperture of the array, the focal spot size, the absorption coefficient, the cavitation threshold and finally the electrical matching of the transducers (linked to ratio between the size of the transducer and the wavelength). On the one hand, at a lower frequency, the absorption coefficient of the brain is smaller and the necrosis threshold would be harder to reach. Moreover the cavitation will appear at lower amplitude since the cavitation threshold increases with frequency. On the other hand, a higher frequency could achieve a more localized focus, but above 1.3 MHz the absorption and the scattering loss of the skull increase rapidly (Fry and Barger 1978), and the acoustic power at focus would not be sufficient. Moreover, at high frequency, the required steering capabilities would be incompatible with a reasonable number of transducers. Finally, contrary to classical HIFU transducers, the single elements technology developed in collaboration with Imasonic presents very good performances in terms of bandwidth since the cut frequencies at  $-6\text{dB}$  are 0.63 MHz and 1.17 MHz. Thus the transducers can be used either in monochromatic or pulse emission mode, for therapeutic or imaging purposes.

In order to optimize the number of transducers and their size, several considerations have been taken into account. The array must be able to focus at its geometric center, correcting the aberrations induced by the skull, so that the active element size has to be smaller than the correlation length of the skull, approximately 10 mm at 1MHz. This has been confirmed by Clement *et al* (2000), since they shown that dividing their large 64 elements array in 500 elements (approximately  $3\text{ cm}^2$ ) working at 650 kHz increased the intensity at focus by a factor 1.5.

Moreover the array must be large enough and distribute energy evenly across the skull bone in order to avoid undesired skull heating. A geometrical focus  $F = 120\text{ mm}$  and an array

diameter  $D = 180$  mm were chosen, minimizing as far as possible the  $F/D$  ratio. Finally, the number of transducers must also be sufficient to deliver therapeutic power level at focus. The acoustic power required in ablation operating regime is typically  $1000 \text{ W.cm}^{-2}$  at  $0.9$  MHz, which corresponds to an overpressure of  $54$  bars at focus after propagation through the skull. Considering the absorption of the brain ( $0.7 \text{ dB.cm}^{-1}.\text{MHz}^{-1}$ ), the reflection and absorption induced by the skull (an average transmission loss of  $11$  dB at  $0.9$  MHz), the overpressure has to reach  $350$  bars at focus in water without the skull. All the transducers of the array have been characterized individually. Each transducer was linked to its  $50$  Ohms electrical matching and the electrical to acoustical efficiency reached  $50\%$ . With a  $16$  W electrical power supply, each transducer could generate a monochromatic wave with amplitude of  $1.8$  bars at  $120$  mm in water during  $5$  seconds. Therefore the array was composed of  $200$  elements.

### **3. Acoustic field simulations**

The performances of several transducers distributions such as quasi-random, annular and hexagonal patterns were investigated (Fig. 1). These specific distributions were chosen for their different degrees of symmetry. The first array consisted of  $200$  elements of  $8$  mm diameter, each distributed in a quasi random manner: a totally random distribution was modified so that the minimum distance between the center of any two neighboring elements was  $10$  mm. The second array was a standard axi-symmetrical array: the elements were regularly placed on concentric rings, each ring being shifted with respect to the others. Finally the hexagonal array was completely regular, and could be easily compared to others hexagonal patterns with any sparseness or hexagonal compact distribution. All the arrays have the same  $52\%$  sparseness, and should provide approximately the same acoustic power at

focus. According to Gavrilov et al. (2000), a sparseness of 52 % being within the limited 40% to 70% range, enabled beneficial effects of randomization.

For each array, the 3D acoustic field was calculated by using the impulse diffraction code PASS<sup>1</sup> (Cassereau and Guyomar 1988). In order to assess the performance of the different arrays, the acoustic fields were calculated when focusing at geometrical focus and when the focus was steered off-axis and along the beam axis. The fields were calculated in a 100x100x200 mm<sup>3</sup> volume with a 0.25 mm step.

The intensity distributions in the focal plane for the hexagonal and quasi-random arrays are shown in Fig. 2. Grating lobes associated with an aperiodic distribution (concentric shifted rings and quasi-random arrays) are 10 to 12dB less than those associated with the periodic hexagonal element spacing array. Actually, the concentric rings array and the quasi-random array have quite similar performance in the focal plane, the maximum grating lobe being lower than -20dB: -22,3dB for the concentric ring array and -21,4dB for the quasi-random array. However the quasi-random array has better performance in the near field: on the beam axis the pressure amplitude of the quasi-random array was found to be 10dB lower than the one of the concentric rings array (Fig. 3). The reduction of the grating lobes in the near field is a very important point to address, as the overheating of the skull surface located in the near field has to be avoided.

The increase of the grating lobes when the focus was electronically moved off-axis has also been investigated. The intensity distributions in the focal plane for the quasi-random array are shown in Fig. 4. On these simulations the focus is steered from 0 to 20 mm off the beam axis. The intensity distribution was deemed acceptable if the maximum pressure in the grating lobes was at least 10 dB lower than the pressure at focus (a factor 10 in the corresponding intensities), which is an accepted level for safe delivery of treatment (Ebbini *et al.* 1991). The

---

<sup>1</sup> <http://www.loa.espci.fr/pass/>.

steering range was found to be very poor with the hexagonal distribution ( $\pm 3$ mm), but quite good with the aperiodic distributions ( $\pm 15$  mm) as it is shown in Fig. 5. Moreover the peak pressure-squared value remains above 50% of its maximum value to a 15 mm steering radial distance and a 20 mm axial distance away from the geometric focus. Thus, treatment volumes of about  $30 \times 30 \times 40 \text{ mm}^3$  should be reached.

Consequently, the quasi-random distribution was definitively chosen as it gives the lowest level of grating lobes in the focal plane as well as in the near field and it presents very good steering capabilities.

## 4. Experiments and results

### 4.1 Array construction

Based on the simulation study a 200-elements array was constructed. The 200 high power piezocomposite transducers (8 mm diameter,  $0.5 \text{ cm}^2$  active area, Imasonic, Besançon, France) were mounted in a sealed spherically curved holder made of a mixture of Ureol 6414B and Ureol 5075A (Vantico Ltd), with a 12 cm radius of curvature. This material was selected for its thermal, mechanical and acoustical properties. Each transducer element is individually matched to the 50 Ohms output impedance of the generator. The matching boxes are placed in a waterproof PVC box (Fig. 6). The coaxial lines from the matching boxes are connected to a 200-channels electronic driving system. Each electronic channel is fully programmable and has its own emission and reception electronic board. 16 electrical Watts per channel ( $\pm 40\text{V}$ , 50 Ohms) can be delivered. A computer is used to control the operation of the 200-channels electronic driving system.

### 4.2 Acoustic field measurements.

The acoustic field was measured at low acoustic intensity ( $< 5 \text{ W.cm}^{-2}$ ) in a tank filled with degassed water. A 0.4 mm PVDF bilaminar calibrated hydrophone (Golden Lipstick, SEA, Soquel, CA) was set at the array geometrical focus. The hydrophone was moved using a stepper-motor-controlled 3D positioning system (Newport). At each location of the hydrophone the measured signal was sent through an amplifier (SEA, Soquel, CA), and recorded by one of the reception channels of the electronic driving system. The scan position and the data acquisition were computer controlled.

A 900 kHz 30 cycles sinusoidal wave was emitted on each channel at low electrical power (0.04 W per channel) and 15 bars were measured at focus. The acoustic field was scanned in a 50x50x50 mm<sup>3</sup> volume with a 0.5 mm step. The experimental fields shown in Fig. 7.a and 7.b are very close to those obtained with the simulation. The -6dB dimension of the focus is 1.5 x 1.5 x 10.5 mm<sup>3</sup>, and the grating lobes are lower than -20 dB.

Then a half human skull was placed between the array and the hydrophone as shown in Fig. 8, the skull-array distance was approximately 4 cm, and the 2D map of the wavefront distortions induced by the skull was recorded. As shown in Fig. 9, the wavefront was severely distorted by the skull. Some part of the skull induced an important phase distortion (the celerity can reach 3500 m.s<sup>-1</sup>), whereas other parts induced a huge absorption (up to 8 dB.mm<sup>-1</sup>). But there is no obvious correlation between the region of high or low attenuation and the region of large or small phase shift. In order to correct for both phase and amplitude aberrations a time reversal process combined with amplitude correction was performed. The signal coming from each transducer of the therapeutic array was recorded by the hydrophone. Then the signals were time-reversed, the amplitudes were adjusted to the same level and the signals were reemitted by the ultrasonic array. This procedure takes advantage of the reciprocity in order to use a sensor rather than an acoustical source at the focus. The resulting acoustic field was scanned in the focal plane. It is shown in Fig. 10 and compared with the field obtained without any aberration corrections. The uncorrected beam is strongly degraded by the skull. The focal spot is not at the desired location and is widely spread in comparison with the corrected one. After correcting the aberrations, the focus is located at exactly the desired position. Moreover, an important point is that the pressure amplitude of the corrected beam (68 Bars) is 4.5 times higher at focus than the pressure amplitude of the uncorrected one (15 bars). Consequently, it results in a 20 times higher heat deposit and it shows the feasibility to induce lesions in the brain.

The time reversal process with amplitude compensation was repeated at several skull positions. The skull was moved step by step in regard to the system array+hydrophone over a few centimeters. For each skull position, the acoustic field was scanned in the focal region. For all locations, thanks to the adaptive focusing the grating lobes were lower than -20 dB, and the -6 dB dimension of focus remained equal to  $1.5 \times 1.5 \times 10.5 \text{ mm}^3$ . The pressure at each focus was also measured and ranged from 52 to 75 bars.

#### *4.3 Thermally induced lesions in fresh tissues with steering process.*

Lesions were induced in fresh degassed liver samples. The temperature of the degassed water was 25 °C. A human skull and a sample of fresh degassed cow liver were set between the array and the hydrophone. The hydrophone was implanted in the tissue sample at the geometrical focus of the array and a time reversal process combined with amplitude compensation was performed. Once the signals had been recorded, the hydrophone was removed. A continuous monochromatic wave with the phase and amplitude previously corrected was emitted on each of the 200 electronic channels. Two sonications were performed at the initial hydrophone location in the liver sample at the maximum power level for a duration of 5s with a waiting time of 10 s between shots. The lesion is about 2 mm in diameter and 8 mm in length. Then, the beam was electronically steered off-axis in order to focus at 8 others points located on a 1-cm side square centered on the geometrical focus. The targets were the four corners and the middle of each side of the square. Two 5s sonications were performed again at each focus, with a waiting time of 10s between each shot. The nine lesions are shown in Fig. 11.a. Due to the change in the liver color, the necroses are very well defined. They are located exactly at the desired position and the boundary between burned cells and other cells is very narrow.

In a second experiment a square-shaped necrosis was created in liver by focusing on 25 points inside of the square with a 2-mm spatial step between each target. Two sonications were performed at each focus for 5s with a waiting time of 10s between shots. As shown in Fig 11.b. the necrosis is a well-defined square of 1.1cm side. The temperature increase has also been modeled by a diffusion type equation computed using the 3D finite-difference time-domain method. The thermal dose for changing temperature exposure was calculated by numerical integration (Sapareto and Dewey 1984). It gives the time that would yield an equivalent thermal dose of 240 min at 43°C and enabled the prediction of the necrosis size in good agreement with the measurements (Fig 11.b).

Finally, a fresh sheep brain was placed behind a half human skull so that the brain surface was located in the focal plane of the system. The hydrophone was implanted in the brain at the geometrical focus of the array and a time reversal process was performed. The aberrations corrections were similar to those of section 4.2. Two sonications of 5 s duration were performed at the geometrical focus. Then the beam was electronically steered in order to focus on a cross centered on the geometrical focus. The beam was steered along a vertical and a horizontal 1cm line with a 0.2mm spatial step, and at each point two 5s sonications were performed. On Fig. 12 the cross-shaped necrosis is well defined although the color change in the brain is not as marked as in the liver.

## **5. Discussion and conclusion**

A large therapeutic array using single-elements technology has been specially designed for transskull brain therapy. Its capabilities in terms of aperture, working frequency, electrical matching and electronic steering have been optimized. The experiments demonstrated that using a time reversal process with amplitude compensation, achieved with an implantable hydrophone, the aberrations induced by the skull are well corrected with this therapeutic

device. A sharp focus was produced at the desired location, and the pressure reaches 4.5 times the pressure obtained with the uncorrected beam. The experiments were repeated at several skull positions and the focusing quality remained very good. Depending on the skull position, the pressure at focus ranged from 52 to 75 bars, which corresponds to an acoustic intensity of 900 to 1900 W.cm<sup>-2</sup>. This is within the range of intensities typically used in ablation operating regimes. The sonication duration can be easily changed in order to induce a thermal dose independent of the skull position.

High power experiments on a large number of *ex-vivo* liver and brain samples have also demonstrated the therapeutic capabilities of the array. Lesions about 2 mm in diameter have been induced after correcting the ultrasound beam. The high precision steering capabilities of the array have also been demonstrated. Electronically steered focusing enables to coagulate tissues through a human skull in a volume of 30 x 30 x 40 mm<sup>3</sup> around the geometrical focus as the acoustic intensity deposit for each individual focus was found to remain higher than 500 W.cm<sup>-2</sup>. Therefore in practice a whole tumor could be treated spot by spot without mechanically moving the system.

The overheating induced on the skull outer table was checked in several locations on the outer table for a 10s sonication time at maximum power (1900 W.cm<sup>-2</sup> at focus) with a 50 % duty cycle. A 2.5 °C spatially averaged temperature increase was found from the initial 25 °C temperature of the water tank. This temperature rise is acceptable (Ter Haar et al., 2002) especially if a water-cooling system is used to reduce the temperature at skin-bone interface.

Another important innovation of this system consists in its electronic driving channels that allow mixing therapeutic and imaging sequences. Each channel is fully programmable and has its own emission and reception electronic board. The transmit and receive sequences can be changed at a very high frame rate. Therefore it could be possible to image the region close

to the focus with the therapeutic array and perform ultrasound based temperature estimation or elastography measurements.

Finally, the single element technology will enable to modify very easily this system by adding additional elements in the array. Thus the power delivered at the focus could be increased and the temperature rise at skin-bone interface could be decreased. This would make it possible to optimize the amplitude compensation technique and fully adjust the amplitude gain of each channel. Moreover the focal spot could be successfully moved in a larger region around the geometrical focus.

### **Acknowledgements**

We would like to thank Imasonic (Besançon, France) for their highly valued collaboration in developing the high power single-element technology. We wish also to thank Didier Cassereau for his help on the impulse diffraction software PASS.

### **References**

- Aubry J-F, Tanter M, Pernot M, Thomas J-L and Fink M 2003 Experimental demonstration of non invasive transskull adaptive focusing based on prior CT scans *J. Acoust. Soc. Am.* **113**, 1, 85-93
- Basauri L and Lele P P 1962 A simple method for production of trackless focal lesions with focused ultrasound : Statistical evaluation of the effects of irradiation on the central nervous system of the cat *J. Physiology* **160** 513-514
- Cassereau D and Guyomar D 1988 Computation of the impulse diffraction of any obstacle by impulse ray modelling – Prediction of the signals distortions *J. Acoust. Soc. Am.* **84** (4) 1504 - 1516
- Chapelon J-Y, Cathignol D, Cain C, Ebbini E, Kluiwstra J, Sapozhnikov O A, Fleury G, Berriet R, Chupin L and Guey J-L 2000 New piezoelectric transducers for therapeutic ultrasound *Ultrasound Med. Biol.*, **26**, 1, 153-159

- Clement GT, White J P and Hynynen K 2000 Investigation of a large area phased array for focused ultrasound surgery through the skull *Phys. Med. Biol.* **45** 1071-1083
- Clement GT, Hynynen K 2000 Criteria for the Design and Characterization of Large-Area Arrays for Transkull Ultrasound Surgery and Therapy *IEEE Ultras Symp.*
- Clement G T, Sun J, Giesecke T and Hynynen K 2000 A hemisphere array for non-invasive brain therapy and surgery *Phys. Med. Biol.* **45** 3707-3719
- Clement GT, Hynynen K 2002 Micro-receiver guided transcranial beam steering *IEEE Trans.Ultrason. Ferroelec. Freq. Contr.* **49** 4 447-53
- Clement GT and Hynynen K 2002 A non-invasive method for focusing ultrasound through the skull *Phys. Med. Biol.* **47** 1219-1236
- Dupenloup F, Chapelon JY, Cathignol D, Sapozhnikov OA. 1996 Reduction of the grating lobes of annular arrays used in focused ultrasound surgery *IEEE Trans. Ultrason., Ferroelect., Freq. Contr.*, **43**, 6, 991–998.
- Dunn F and Fry F 1971 Ultrasonic threshold dosages for the mammalian central nerveous system *IEEE Trans. Biomed. Eng* **18** 253-256
- Ebbini E, Cain C, 1991 A spherical-section ultrasound phased-array applicator for deep localized hyperthermia, *IEEE Trans. Biomed. Eng* **38** 634-643
- Fry F J and Barger J E 1978 Acoustical properties of the human skull *J. Acoust. Soc. Am.* **63** 1576-1590
- Fry F J, Sanghvi N T, Morris R F, Smithson S, Atkinson L, Dines K, Franklin T, Hastings J 1986 A focused ultrasound system for tissue volume ablation in deep seated brain sites *IEEE Proc. Ultras. Symp*
- Gavrilov L and Hand J 2000 A theoretical assessment of the relative performance of spherical phased arrays for ultrasound surgery *IEEE Trans.Ultrason. Ferroelec. Freq. Contr.* **47** 1 125-138
- Goss J A, Frizzell L A, Kouzmanoff J T, Barich J M and Yang J M 1996 Sparse random ultrasound phased array for focal surgery *IEEE Trans.Ultrason. Ferroelec. Freq. Contr.* **43** 6 1111-1121
- Hynynen K, Jolesz FA 1998 Demonstration of potential noninvasive ultrasound brain therapy through an intact skull *Ultrasound Med. Biol.* **24** 275-83
- Lockwood G R and Foster F S 1996 Optimizing the radiation pattern of sparse periodic two-dimensional arrays *IEEE Trans. Ultrason., Ferroelect., Freq. Contr.* **43** 15–19
- Pernot M, Aubry J-F, Tanter M, Thomas J-L and Fink M 2001 Experimental validation of finite differences simulations of the ultrasonic wave propagation through the skull *IEEE Proc. Ultras. Symp*

- Robinson T C and Lele P P 1972 An analysis of lesion development in the brain and in plastics by high-intensity focused ultrasound at low-Megahertz frequencies *J. Acoust. Soc. Am.* **51** 1333-1351
- Sapareto S and Dewey W 1984 Thermal dose determination in cancer therapy *Int. J. Radiation Oncology Biol. Phys.* **10** 787-800
- Sun J and Hynynen K 1998 Focusing of therapeutic ultrasound through a human skull: a numerical study *J. Acoust. Soc. Am.* **51** 1333-1351
- Smith S W, Trahey G E, Von Ramm O T, 1986 Phased array ultrasound imaging through planar tissue layers *Ultrasound Med. Biol.* **12** 229-243
- Tanter M, Thomas J L and Fink M 1998 Focusing and steering through absorbing and aberrating layers : application to ultrasonic propagation through the skull. *J. Acoust. Soc. Am.* **103** 2403-2410
- Ter Haar G, Kennedy J and Wu F 2002 HIFU Treatments : Dosimetric considerations. *Proceedings of the 2<sup>nd</sup> International Symposium on Therapeutic Ultrasound*, Seattle, 307-313.
- Thomas J L and Fink M 1996 Ultrasonic beam focusing through tissue inhomogeneities with a time reversal mirror : application to transskull therapy *IEEE Trans. Ultrason. Ferroelec. Freq. Contr.* **43** 1122-1129
- Vykhodtseva N I, Hynynen K and Damianou C 1994 Pulse Duration and Peak intensity during focused ultrasound surgery : theoretical and experimental effects in rabbit brain in vivo, *Ultrasound Med. Biol.* **20** 987-1000
- White D N, Clark JM, White DA, Campbell JK, Bahuleyan K, Kraus AS, Brinker RA 1969 The deformation of ultrasonic field in passage across the living and cadaver head *Med. Biol. Engng.* **7** 607-618

## Figure captions

Fig. 1. (a) Hexagonal (b) annular and (c) quasi-random transducer distributions.

Fig. 2. Pressure distribution in the focal plane for the hexagonal (left) and quasi-random (right) arrays. The pressure squared is in dB scale.

Fig. 3. Maximum pressure squared (in dB scale) reached on the beam axis for the concentric ring and quasi random arrays.

Fig. 4. Intensity distribution in the focal plane for the quasi-random array, with the focus moved electronically at (a) 0 mm (b) 5mm (c) 10mm and (d) 15 mm in the y lateral direction.

Fig. 5. Maximum intensity of the grating lobes when the focus is steered from 0 to 20 mm off the beam axis. The values are normalized by the intensity of the main lobe. Solid line : quasi random array. Dotted line : annular array. Dash-dotted line : hexagonal array.

Fig. 6. The 200-element sparse array prototype and the electronic system. The waterproof PVC cube contains the 200 electrical matching boxes. On the right : the quasi random distribution of transducers embedded in spherical shaped Ureol.

Fig. 7. (a) Experimental scan of the pressure squared for the quasi-random array in the focal plane (XY plane). This beam pattern was found to be in good agreement with the numerical simulation in Fig. 4. (b) Experimental scan of the pressure squared in the longitudinal XZ plane. The white lines correspond to  $-3\text{dB}$  and  $-6\text{dB}$ .

Fig. 8 Experimental setup for the time reversal process. On the left side : the needle hydrophone (PZT, 0.4 mm, SEA) used for the corrections of the skull aberrations. On the right side : the high power 200-elements ultrasonic array. The whole experiment is performed in degassed water.

Fig. 9. 2D spatial map of the wavefront aberrations induced by the skull. Typically the celerity in the skull can reach  $3500\text{ m}\cdot\text{s}^{-1}$  in some locations and the absorption  $8\text{ dB}\cdot\text{mm}^{-1}$ . The black dots represents the projection of the transducers positions. (a) The phase distortions ( $\mu\text{s}$ ) (b) The relative amplitude distortion.

Fig. 10. Experimental distribution of the intensity in the focal plane (a) without aberrations corrections and (b) with corrections. Black lines correspond to  $-3\text{ dB}$ ,  $-6\text{ dB}$  and  $-9\text{ dB}$ .

Fig. 11. Thermally induced lesions in fresh liver through a human skull. The target is located at depth  $Z = 120\text{ mm}$  from the array. In both experiments the aberration corrections were achieved at center by using an implanted hydrophone and the other impacts were achieved by tilting electronically the beam. a) Lesion size is about 2 mm in diameter for the center spot. The spatial step between each lesion is 5 mm. b) Square-shaped necrosis performed with 25 electronically steered focus (2mm spatial step). The thermal dose has been calculated for this

experiment. The contour delimits the zone where the thermal dose is higher than 243 min. It predicts the size of the necrosis in good agreement with the real necrosis.

Fig. 12. Thermally induced lesions in a sheep brain through a human skull. The target is located at depth  $Z = 120$  mm from the array. The aberration corrections were achieved at center by using an implanted hydrophone and next impacts were achieved by tilting electronically the beam along a cross. On the vertical and the horizontal lines the step between each lesion was 0.2 mm. The white arrows point the extremity of the cross.

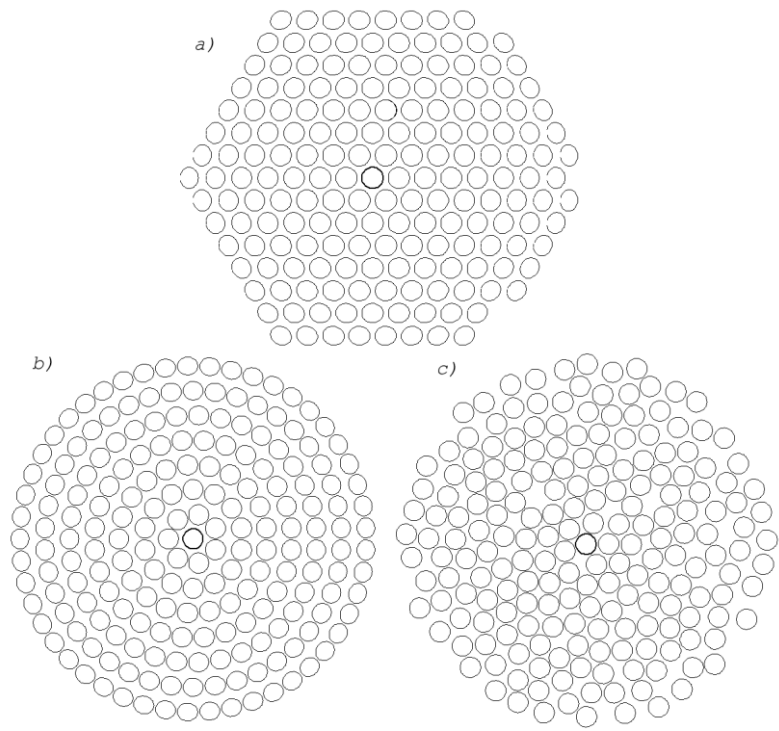


Figure 1

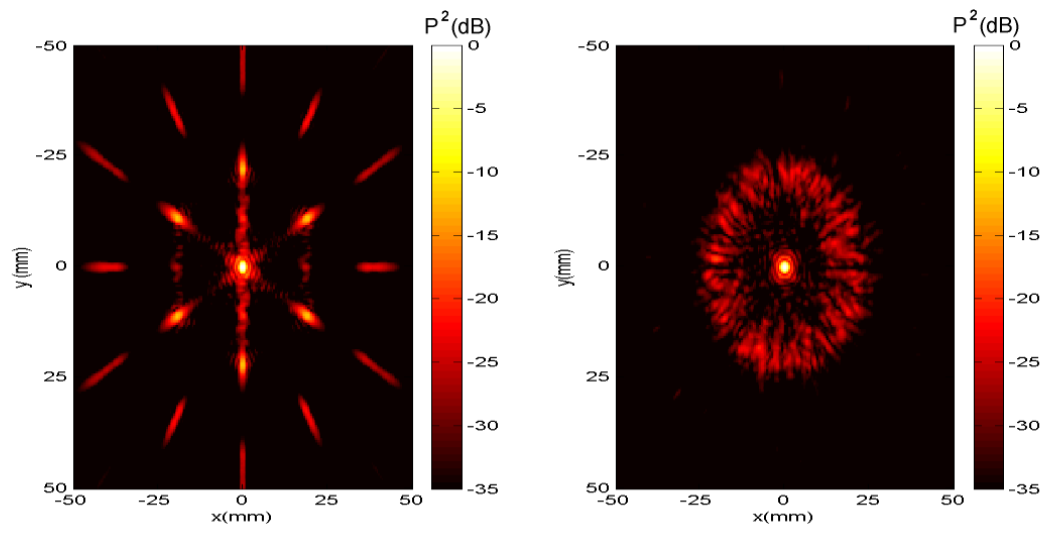


Figure 2

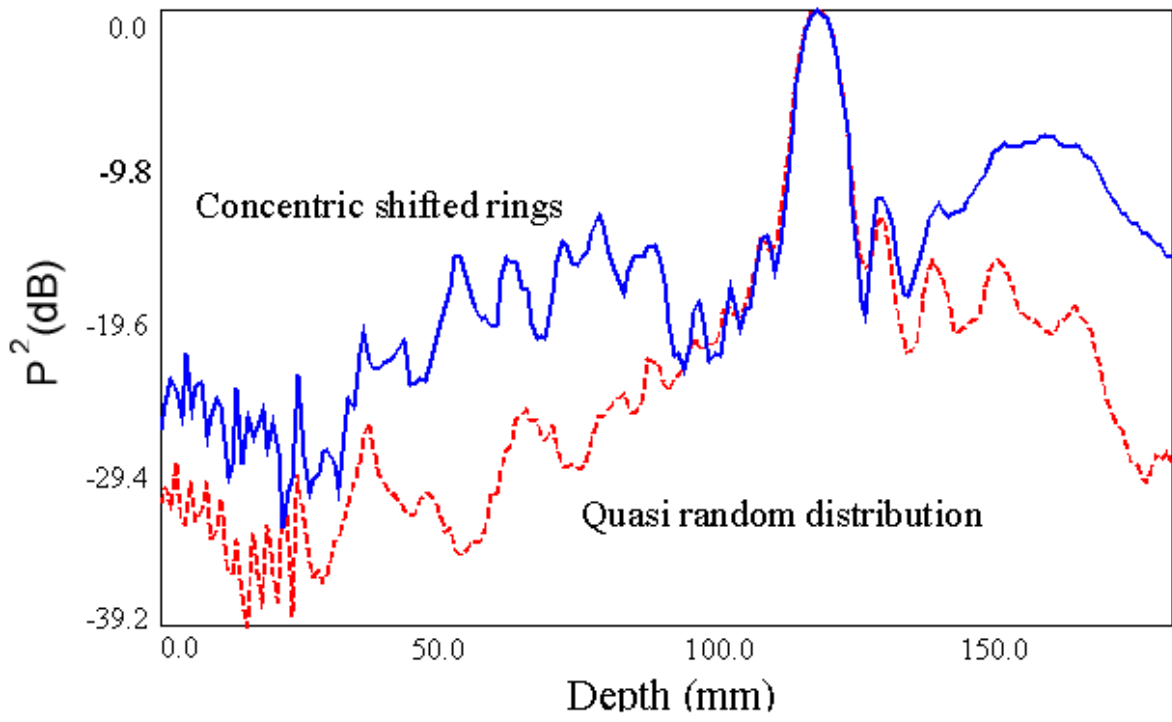


Figure 3

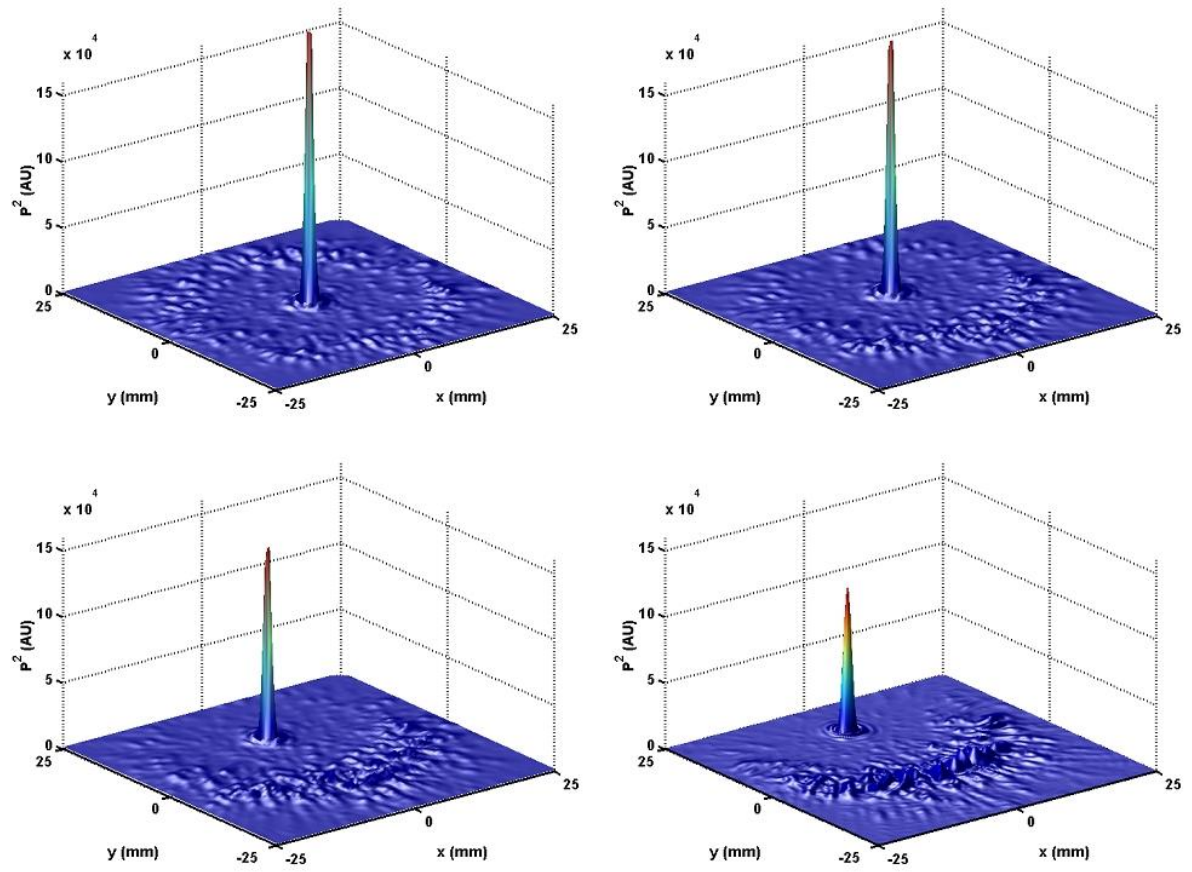


Figure 4

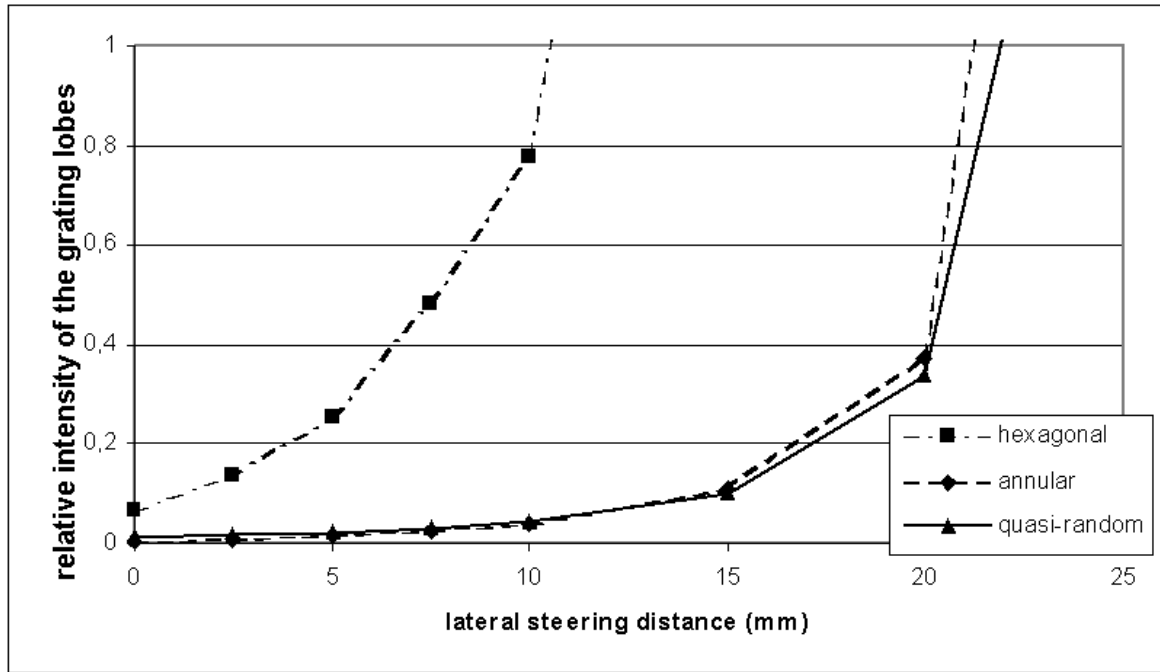


Figure 5



Figure 6

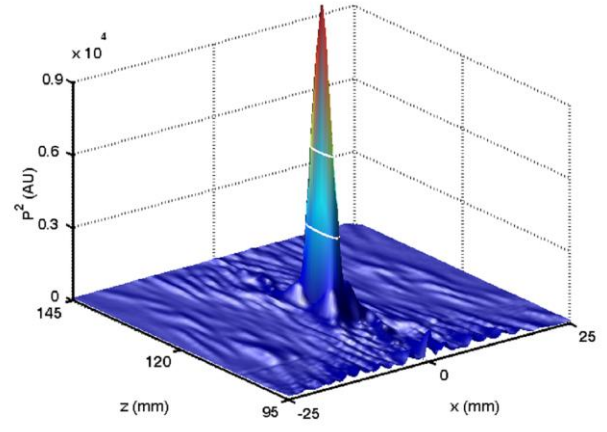
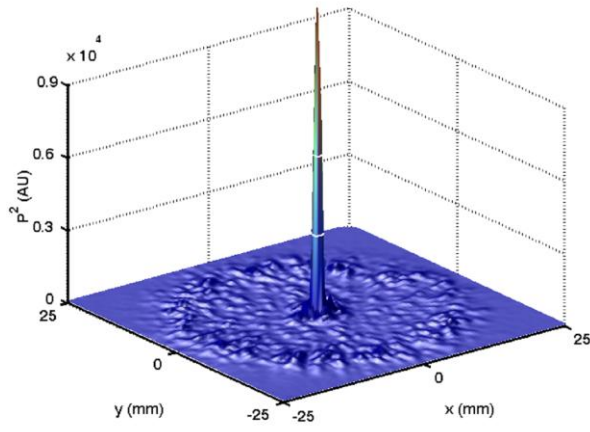


Figure 7

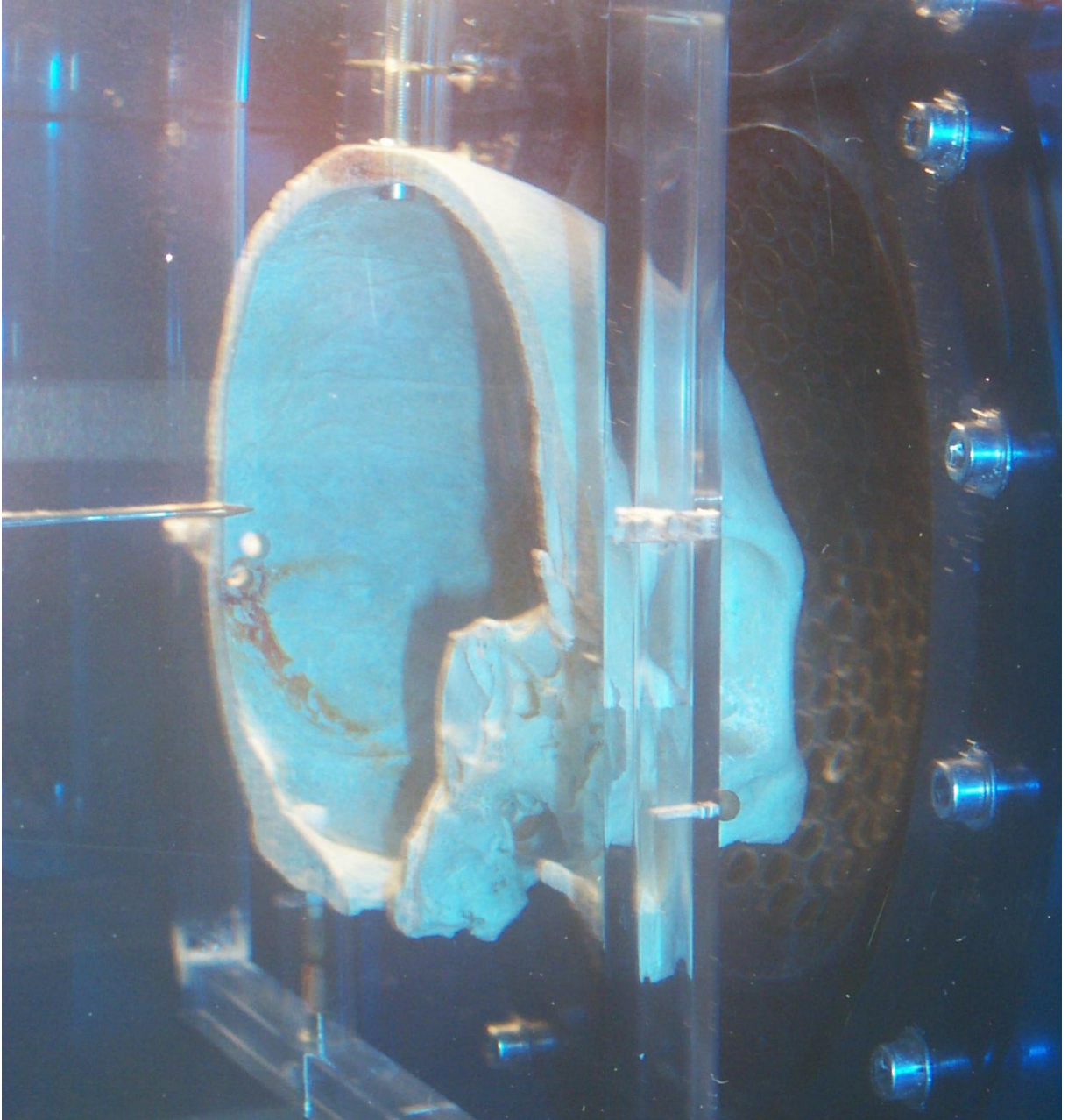


Figure 8

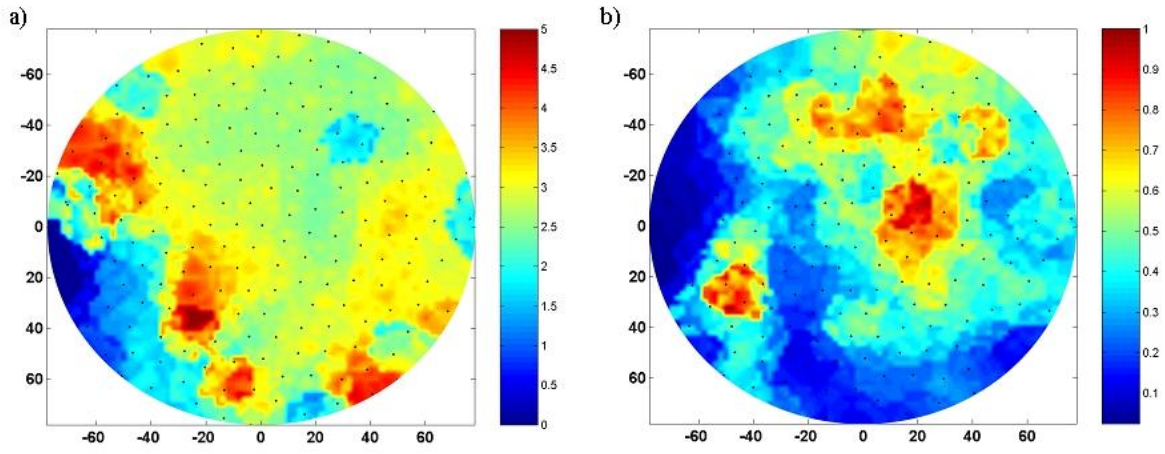


Figure 9

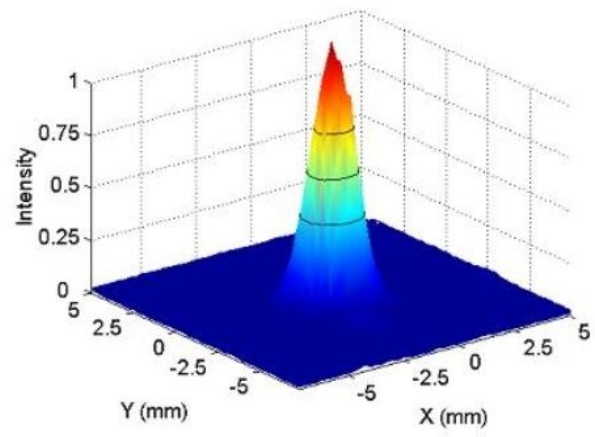
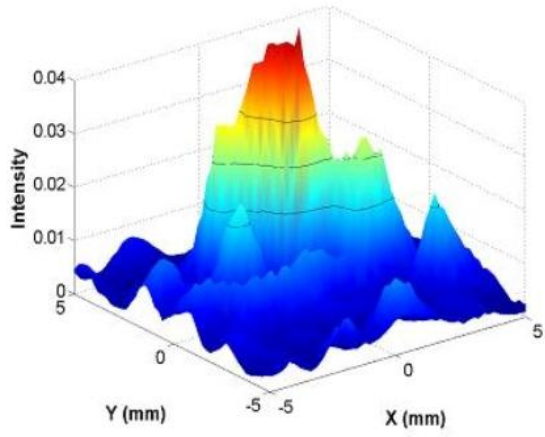


Figure 10

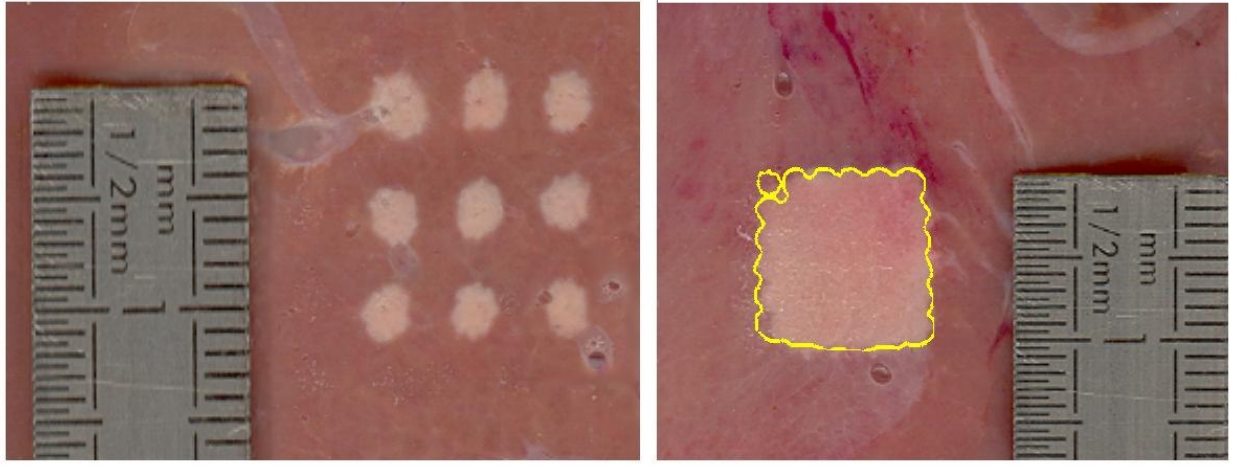


Figure 11

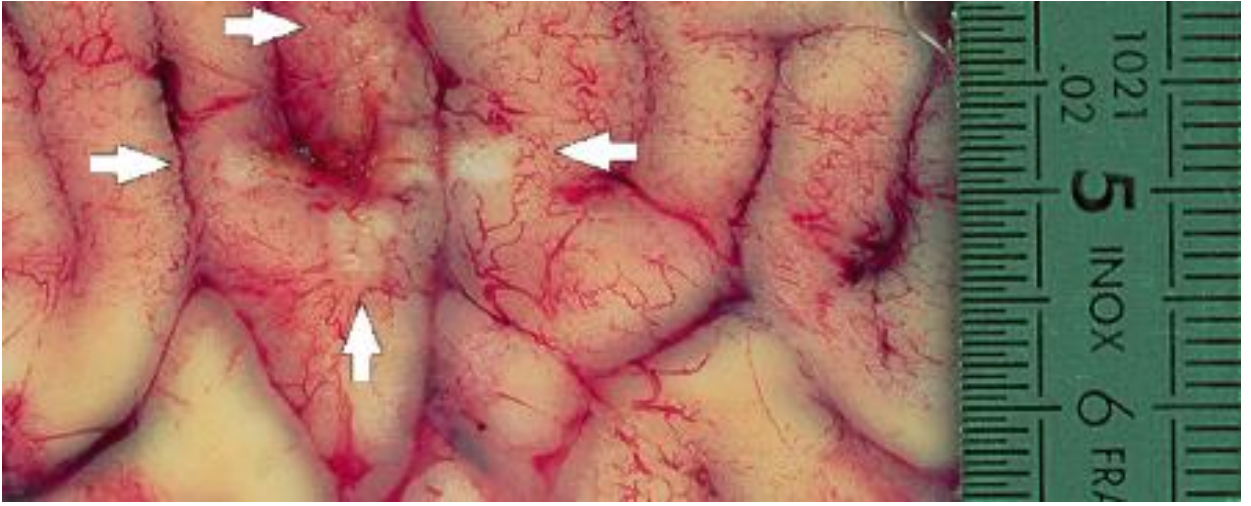


Figure 13